Materials Science & Engineering A 564 (2013) 130–139

Contents lists available at SciVerse ScienceDirect

Materials Science & Engineering A

journal homepage: www.elsevier.com/locate/msea

Effect of iron on the microstructure and mechanical property of Al–Mg–Si–Mn and Al–Mg–Si diecast alloys

Shouxun Ji*, Wenchao Yang, Feng Gao, Douglas Watson, Zhongyun Fan

Brunel Centre for Advanced Solidification Technology (BCAST), Brunel University, Uxbridge, Middlesex, UB8 3PH, UK

ARTICLE INFO

Article history:
Received 30 July 2012
Received in revised form
20 October 2012
Accepted 26 November 2012
Available online 1 December 2012

Keywords:
Aluminium alloy
Mechanical properties
Fe-rich compounds
High pressure die casting
CALPHAD

ABSTRACT

Al–Mg–Si based alloys can provide super ductility to satisfy the demands of thin wall castings in the application of automotive structure. In this work, the effect of iron on the microstructure and mechanical properties of the Al–Mg–Si diecast alloys with different Mn concentrations is investigated. The CALPHAD (acronym of Calculation of Phase Diagrams) modelling with the thermodynamic properties of the multi-component Al–Mg–Si–Mn–Fe and Al–Mg–Si–Fe systems is carried out to understand the role of alloying on the formation of different primary Fe-rich intermetallic compounds. The results showed that the Fe-rich intermetallic phases precipitate in two solidification stages in the high pressure die casting process: one is in the shot sleeve and the other is in the die cavity, resulting in the different morphologies and sizes. In the Al–Mg–Si–Mn alloys, the Fe-rich intermetallic phase formed in the shot sleeve exhibited coarse compact morphology and those formed in the die cavity were fine compact particles. Although with different morphologies, the compact intermetallics were identified as the same α-AlFeMnSi phase with typical composition of $Al_{24}(Fe,Mn)_6Si_2$. With increased Fe content, β-AlFe was found in the microstructure with a long needle-shaped morphology, which was identified as $Al_{13}(Fe,Mn)_4Si_{0.25}$. In the Al–Mg–Si alloy, the identified Fe-rich intermetallics included the compact α-AlFeSi phase with typical composition of Al_8Fe_2Si and the needle-shaped β-AlFe phase with typical composition of $Al_{13}Fe_4$. Generally, the existence of iron in the alloy slightly increases the yield strength, but significantly reduces the elongation. The ultimate tensile strength maintains at similar levels when Fe contents is less than 0.5 wt%, but decreases significantly with the further increased Fe concentration in the alloys. CALPHAD modelling shows that the addition of Mn enlarges the Fe tolerance for the formation of α-AlFeMnSi intermetallics and suppresses the formation of β-AlFe phase in the Al–Mg–Si alloys, and thus improves their mechanical properties.

1. Introduction

In Al–Mg–Si based alloys that can provide super ductility in castings [1], iron is a common impurity element but it is unavoidably picked up during melting and casting, and particularly when the scraped and recycled materials are used. Although the presence of iron is beneficial to prevent die soldering in high pressure die casting (HPDC) process [2,3], the excessive iron has been found to be detrimental to the mechanical properties of Al–Si, Al–Si–Cu and Al–Si–Mg alloys [4,5]. Generally, the effect of Fe-rich phases on the mechanical properties of aluminium alloys depends on their type, size and amount in the microstructure.

A variety of Fe-rich intermetallic phases have been observed in aluminium alloys. In Al–Si–Fe system there are five main Fe-rich phases: Al_3Fe (or $Al_{13}Fe_4$), α-Al_8Fe_2Si (possibly α-$Al_{12}Fe_3Si_2$), β-Al_5FeSi, δ-Al_4FeSi_2 and γ-Al_3FeSi [6,7]. Among them, β-Al_5FeSi usually appears as highly faceted platelets up to several millimetres and it therefore causes the most serious loss of strength and ductility in the castings [8,9]. However, the α-Al_8Fe_2Si phase has been reported as the compounds with many different types of morphology [10,11]. The morphological changes from plate to Chinese script or compact shapes were reported to enhance mechanical properties [12,13]. On the other hand, manganese has been widely used to suppress the development of long needle-shaped Fe-rich phases and to promote the formation of compact Fe-rich phases in aluminium alloys [14]. In hypoeutectic Al–Si alloys containing Fe, Mn and Mg, three Fe-rich phases of α-$Al_{15}(FeMn)_3Si_2$, β-Al_5FeSi and π-$Al_8FeMg_3Si_6$ compounds have been identified [8,15]. In the commonly used Al–Si–Mg cast alloys, with a Mn/Fe ratio of 0.5, the structure of Fe-rich intermetallics is body centred cubic α-$Al_{15}(FeMn)_3Si_2$ [16,17], which may appear as hexagonal, star-like, or dendritic crystals at different Mn/Fe ratios [18]. However, in the various results from previous studies, the effect of Fe on the microstructure is in good

* Corresponding author. Tel.: +44 1895 266663; fax: +44 1895 269758.
E-mail address: shouxun.ji@brunel.ac.uk (S. Ji).

0921-5093
http://dx.doi.org/10.1016/j.msea.2012.11.095

agreement in the most popular Al–Si cast alloys, but it is inconsistencies for the influence of Fe on the mechanical properties of castings [13]. Meanwhile, the amount of Mn needed to neutralize Fe has not been well established [19,20]. Although Mn/Fe ratio of 0.5 is desirable for the transformation of β-Al_5FeSi to α-$Al_{15}(FeMn)_3Si_2$ [13].

The formation of Fe-rich intermetallics is greatly affected by solidification conditions during casting [21,22]. The superheat and cooling rate have been reported to affect the nucleation and growth of the Fe-rich phases and thus to be able to modify the morphology and size of the intermetallics in aluminium alloys [23,24]. At high cooling rates as in the case of HPDC, the occurrence of primary β-AlFeSi needles is shifted towards higher iron levels at Fe > 1% [25,26]. These observations are important in understanding the microstructure features of Al–Si and Al–Si–Cu cast alloys. However, insight in solidification of other alloys is still limited in terms of the Fe-rich intermetallic phases at different contents of Fe and Mn, especially under high cooling rate with HPDC process. Meanwhile, the thermodynamic modelling by CALPHAD is becoming an important tool in alloy development, which can determine the phase formation under the equilibrium condition. The thermodynamic modelling of Al–Fe–Mn–Si system has been carried out by Balitchev et al. [27]. They achieved reasonably good results by treating the α-AlFeMnSi phase as a stoichiometric compound. The similar approaches were also used by Fang et al. [28] for the formation of Fe-rich intermetallics in semisolid processed A380 and A356 alloys. These results provided a guideline for understanding the solidification and phase formation process. Therefore, the further investigation for the phase formation of Fe-rich intermetallics in the diecast Al–Mg–Si (–Mn) alloys is necessary in order to enhance the understanding towards the integration of thermodynamics, solidification and microstructural evolution, and mechanical properties. This is practically important in materials recycling where the various elements and the different amount of corrector elements are required during casting.

The present study attempts to investigate the effect of Mn and Fe on the morphology, size and distribution of various Fe-rich compounds in the Al–Mg–Si alloy produced by HPDC process. The mechanical properties of yield strength, ultimate tensile strength and elongation were assessed with different Fe and Mn contents. The role of alloy chemistry on the effect of Fe and Mn was investigated by CALPHAD modelling of multi-component Al–Mg–Si–Mn–Fe and Al–Mg–Si–Fe systems. The thermodynamic modelling and the experimental findings of the Fe-rich intermetallic compounds were studied with respect to the role of Mn on combating the detrimental effect of Fe in the Al–Mg–Si alloy. The discussions are focused on the phase formation of different Fe-rich intermetallic phases and the relationship between Fe-rich compounds and mechanical properties of the diecast Al–Mg–Si alloys.

2. Experimental

The Al–Mg–Si alloys with different Fe and Mn contents were produced by melting the ingots of commercial pure aluminium, pure magnesium and the master alloys of Al-15 wt%Si, Al-20 wt%Mn, Al-10 wt%Ti and Al-80 wt%Fe. During the experiments, each element was weighed to a specified ratio with different extra amounts for burning loss compensation during melting. The 6–10 kg melt was prepared in a clay-graphite crucible using an electric resistance furnace. The processing temperature of the melt ranged between 690 and 750 °C. For all the experiments, the melt was subjected to fluxing and degassing using commercial fluxes and N_2. The N_2 degassing usually lasted 3 min and the granular flux covered on the top surface of the melt during N_2 degassing. The sample for composition analysis was taken from the melt after homogenisation.

A $\phi 40 \times 60$ mm cylindrical sample was made by casting the melt directly into a steel mould for the composition analysis. The casting was cut across the diameter at 15 mm from the bottom and ground down to 800 grid abrasive grinding paper. The composition of each alloy was obtained from an optical mass spectroscopy, in which at least five spark analyses were performed and the average value was taken as the chemical composition of alloy. The composition was further confirmed by area energy dispersive X-ray (EDX) quantification in SEM. The actual compositions of the alloys containing 0.02 wt% and 0.54 wt% Mn are shown in Table 1.

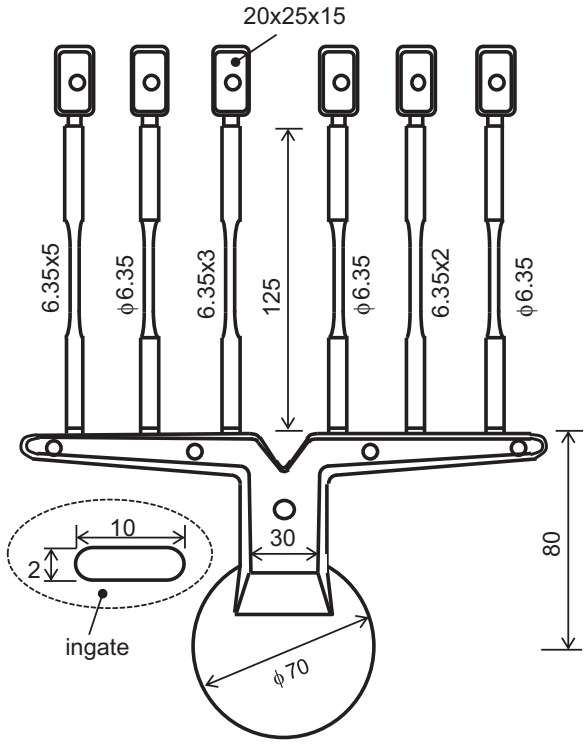

Fig. 1. Diagram of die castings for the standard tensile testing samples of cast aluminium alloy according to the specification defined in ASTM B557-06. The overflow and biscuit are designed in associated with cold chamber die casting machine. The dimensions are in mm.

Table 1
Compositions of diecast Al–Mg–Si alloys used in experiments (wt%).

Alloy	Si	Fe	Mn	Mg	Ti	Zn	Others	Al
A	2.2 ± 0.08	varied*	0.541 ± 0.05	6.2 ± 0.08	0.17 ± 0.04	0.012 ± 0.004	< 0.03	Bal.
B	1.9 ± 0.07	varied[a]	0.023 ± 0.04	5.6 ± 0.09	0.15 ± 0.04	0.013 ± 0.004	< 0.03	Bal.

* Actual Fe contents were measured to be 0.214, 0.389, 0.623, 0.841, 1.243, 1.490, 1.861, and 2.482, respectively.
[a] Actual Fe contents were measured to be 0.086, 0.414, 0.634, 0.911, 1.188, 1.420, 1.542, and 1.821, 2.453, respectively.

After composition analysis and skimming, the melt was manually dosed and subsequently released into the shot sleeve of a 4500 kN HPDC machine for the final casting, in which all casting parameters were fully monitored. The pouring temperature was measured by a K-type thermocouple, usually at 50 °C above the liquidus of the alloy according to the equilibrium phase diagram. Six ASTM standard samples with three ϕ6.35 mm round bar and three square bar were cast in each shot. The diagram of die castings for the standard tensile testing samples is shown in Fig. 1. The casting die was heated by the circulation of oil at 250 °C. All castings were kept at ambient condition for at least 24 h before the mechanical property test.

The tensile tests were conducted following the ASTM B557 standard using an Instron 5500 Universal Electromechanical Testing Systems equipped with Bluehill software and a ±50 kN load cell. All the tests were performed at ambient temperature (~25 °C). The gauge length of the extensometer was 25 mm and the ramp rate for extension was 2 mm/min. Each data reported is

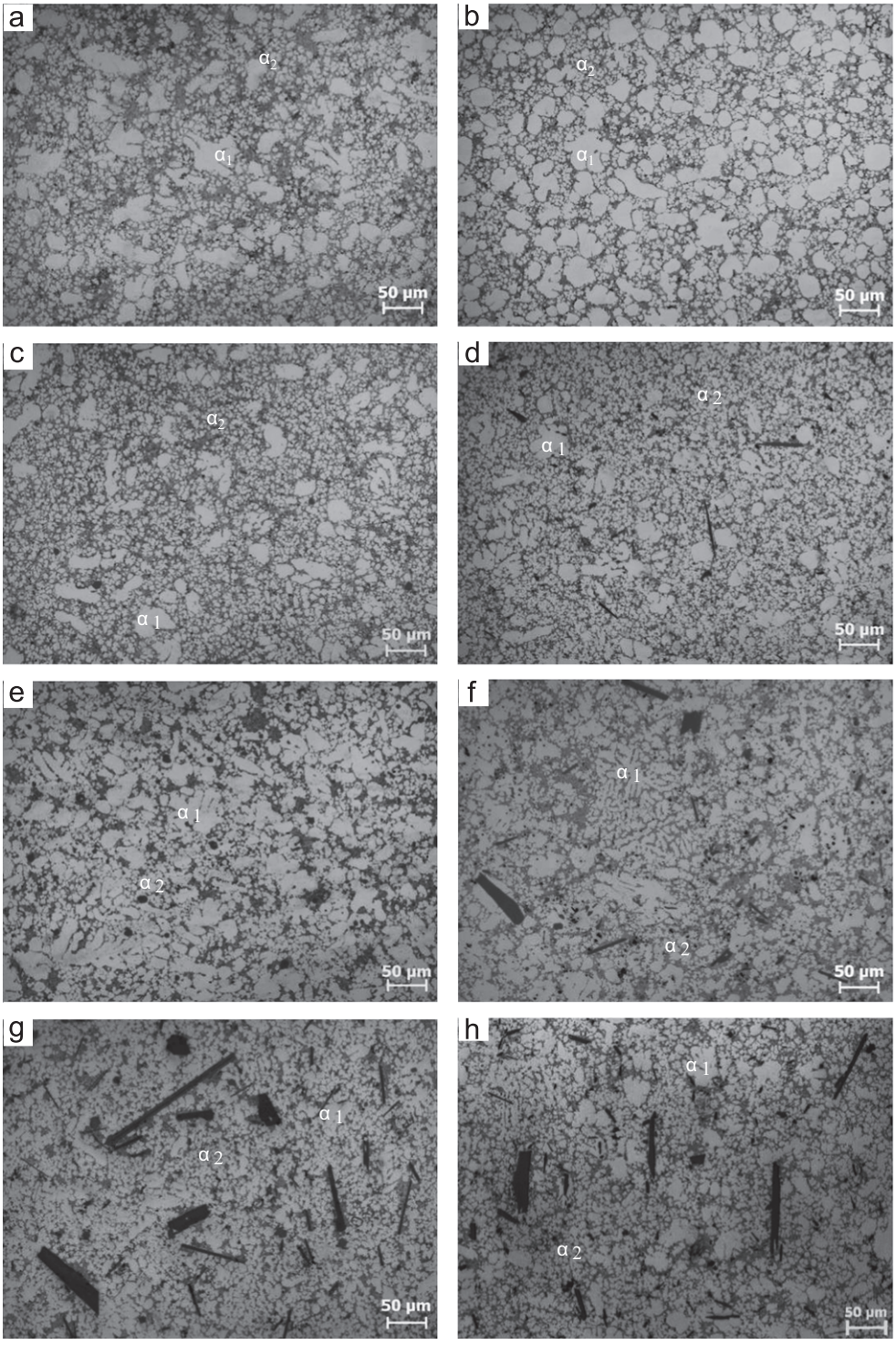

Fig. 2. Optical micrographs showing the microstructure of diecast alloy with different amounts of Fe and Mn, (a) 0.54Mn, 0.21Fe, (b) 0.02Mn, 0.09Fe, (c) 0.54Mn, 0.62Fe, (d) 0.02Mn, 0.63Fe, (e) 0.54Mn, 1.24Fe, (f) 0.02Mn, 1.19Fe, (g) 0.54Mn, 1.86Fe, (h) 0.02Mn, 1.82Fe.

based on the properties obtained from 10 to 30 samples without showing obvious casting defects on the fractured surfaces.

The specimens for microstructure examination were cut from the middle of ϕ6.35 mm round tensile test bars. The microstructure was examined using a Zeiss optical microscopy with quantitative metallography, and a Zeiss SUPRA 35VP scanning electron microscope (SEM), equipped with EDX. The particle size, volume fraction and the shape factor of the solid phase were measured using an AxioVision 4.3 Quantimet digital image analysis system. The quantitative EDX analysis in SEM was performed at an accelerating voltage of 20 kV on a polished sample, and the libraries of standard X-ray profiles for EDX were generated using pure elements. In situ spectroscopy calibration was performed in each session of the EDX quantification using pure copper. To minimise the influence from the interaction volume during the EDX quantification, five point analyses on selected particles were conducted for each phase and the average was taken as the measurement.

3. Results

3.1. As-cast microstructure of the diecast Al–Mg–Si alloys

In the as-cast state, there was no significant change in the morphologies of the primary α-Al phase and eutectic phase presented in the Al–Mg–Si alloys containing different levels of Fe and Mn. However, the primary α-Al solid solution was found in two types of morphology in each alloy, which are labelled as 'α_1' and 'α_2' in Fig. 2, respectively. The α_1-Al phase was formed in the shot sleeve, in which the cooling rate is up to 10^2 K/s during solidification. This resulted in the formation of dendrites and fragmented dendrites in the microstructure. The α_2-Al phase was believed to be formed in the die cavity under a cooling rate over 10^3 K/s during solidification, which showed fine globular morphology in the microstructure. The sizes of dendritic and fragmented dendritic α_1-Al phase ranged from 20 to 100 μm and the fine globular α_2-Al particles ranged from 3 to 20 μm. The coarse α_1-Al phase was isolated by fine globular α_2-Al particles. The interdendritic regions were characterised with a eutectic microstructure (labelled as 'E' in Fig. 3), in which the lamellar structure was made of α-Al and Mg_2Si phases. The primary α-Al phase was associated with the eutectic microstructure. Fe-rich intermetallic compounds were observed in the eutectic areas. In order to simplifying the explanation, the solidification in the shot sleeve is described as first solidification and the solidification in the die cavity is described as secondary solidification.

In contrast to the primary α-Al phase, it is seen that the effect of Fe and Mn on the morphologies of primary Fe-rich compounds was significant. Different types and amounts of the Fe-rich intermetallics were related to the Fe and Mn contents, as shown in Figs. 2 and 4. From the experimental observations, only a small amount of fine intermetallic compounds were present in the alloys that contain up to 0.21 wt%Fe (Figs. 2 and 4a and b). The fine Fe-rich intermetallics were formed in the secondary solidification inside the die cavity (labelled as 'Fe_2' in Fig. 4). Most of the fine intermetallics were located between the primary α-Al phase (α_1-Al and α_2-Al), although some intermetallics were found inside them. No primary Fe-rich intermetallic compounds were observed in the primary α-Al phase precipitated in the first solidification. The EDX quantitive analysis by SEM identified the Fe-rich phase with the typical composition of the α-$Al_{24}(Fe,Mn)_6Si_2$ phase in the Al–Mg–Si alloy with Mn addition and the α-Al_8Fe_2Si phase in the Al–Mg–Si alloy without Mn addition. No β-AlFe and β-AlFeSi intermetallics were observed in the samples at this composition.

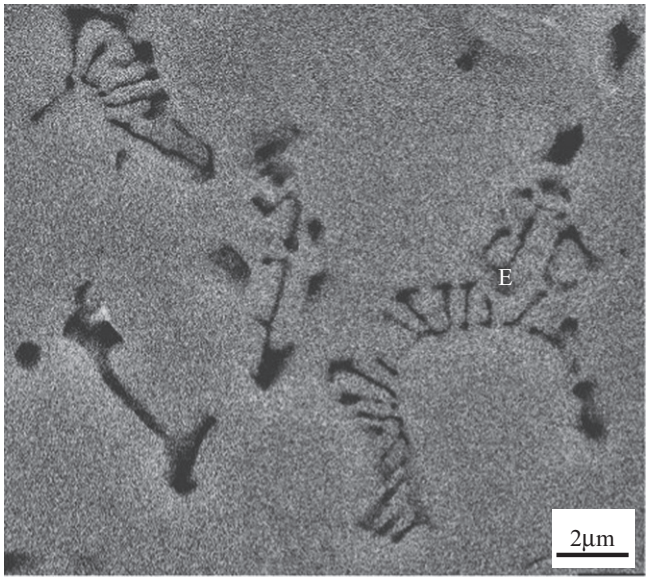

Fig. 3. SEM micrograph showing the typical microstructure of eutectic Al–Mg_2Si phase in the diecast Al–5Mg–2Si alloys.

When the Fe contents in the alloys were increased to a level of 1.2 wt%Fe, there were two types of Fe-rich intermetallics observed. In the Al–Mg–Si alloy with Mn addition (Fig. 4c and d, e and f), the Fe-rich intermetallics were formed in both the first solidification and the secondary solidification, which were labelled as 'Fe_1' and 'Fe_2', respectively. The Fe_1-rich intermetallics were usually associated with the primary α_1-Al phase and exhibited coarse compact morphology, which were found in tetragonal, pentagonal, hexagonal shapes. EDX quantification has identified the Fe-rich intermetallics to be the α-AlFeMnSi phase with the typical composition of α-$Al_{24}(Fe,Mn)_6Si_2$. Meanwhile, the fine intermetallics (labelled as Fe_2) were associated with α_2-Al phase and segregated in the primary α-Al grain boundaries, which were identified by EDX quantification to be the same α-AlFeMnSi phase with the typical composition of α-$Al_{24}(Fe,Mn)_6Si_2$. In the Al–Mg–Si alloy without Mn addition (Fig. 4d and f), the fine Fe-rich phase was also found at the primary α-Al grain boundaries, which exhibited similar morphology and size to that in the alloy with Mn addition. The fine Fe-rich intermetallic phase was identified as the α-AlFeSi phase with the typical composition of α-Al_8Fe_2Si. However, the primary Fe-rich phase formed in the first solidification showed very different morphology in comparison with that formed in the alloy with Mn addition. As seen in Fig. 4d and f, the Fe_1-rich phase exhibited needle-shaped morphology, which crossed through both the primary α-Al phases formed in the first solidification and the secondary solidification. The EDX quantification confirmed that the needle-shaped Fe-rich phase was β-AlFe phase with the typical composition of β-$Al_{13}Fe_4$. It is clearly seen that the additions of Mn can extent the range of Fe contents to form α-AlFeMnSi phase in the alloys. In other words, the Fe content to initialize the β-AlFe phase is increased by adding Mn in the alloys.

When the Fe contents in the alloys was further increased to a level of 1.8 wt% in Al–Mg–Si–Mn–Fe and Al–Mg–Si–Fe systems. In the Al–Mg–Si alloy with Mn addition, as shown in Fig. 4g, a large fraction of long needle-shaped Fe-rich intermetallics were found in the microstructure (bright strip in Fig. 4g), in addition to the compact Fe-rich phase. The coarse and the fine compact primary Fe-rich intermetallics were identified by EDX quantification as the α-AlFeMnSi phase with the typical formula of α-$Al_{24}(Fe,Mn)_6Si_2$. The long needle-shaped Fe-rich compounds were quantitively

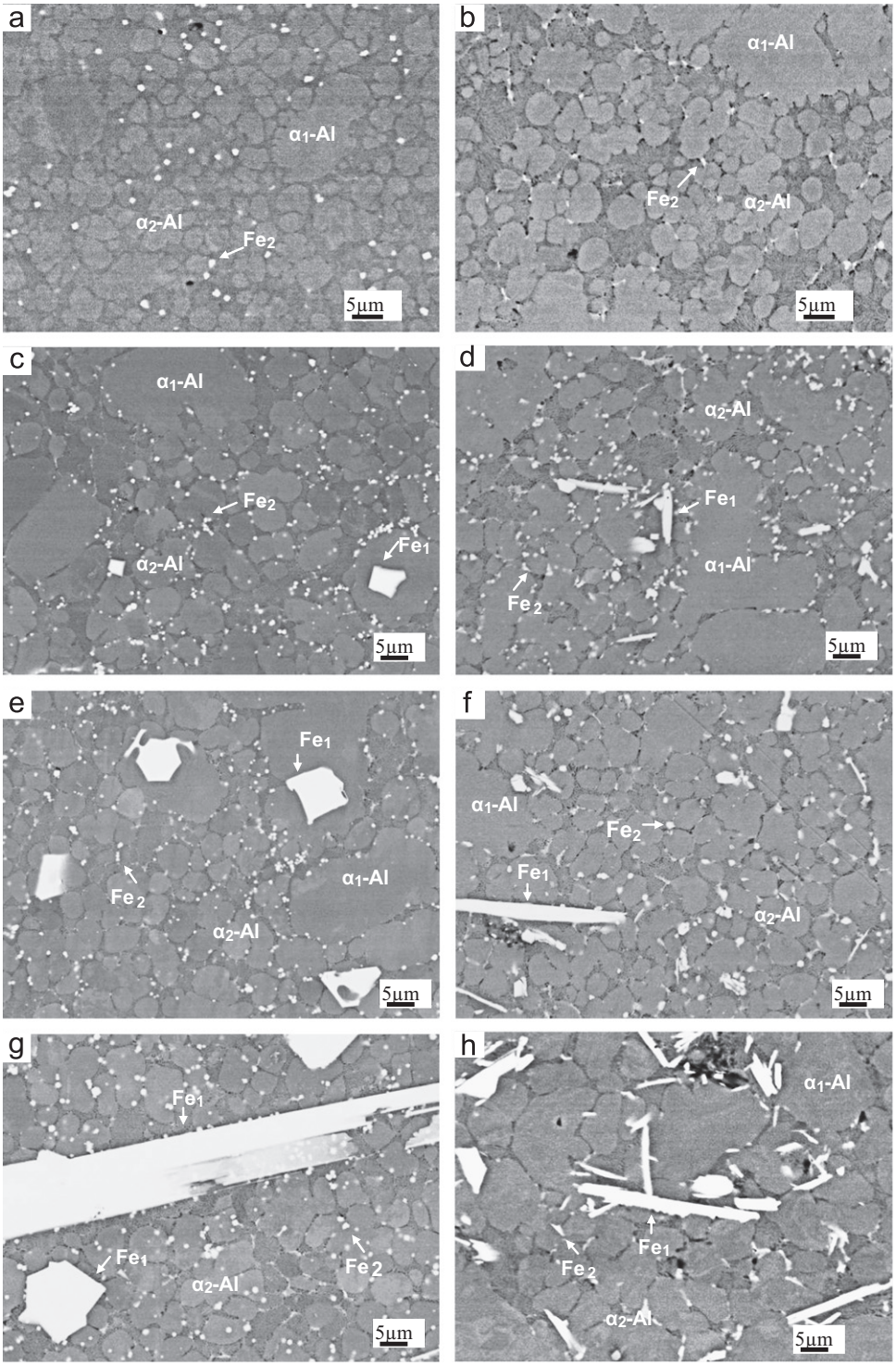

Fig. 4. Backscattered SEM micrographs showing the morphology of Fe-rich intermetallics in the diecast alloy with different amounts of Fe and Mn, (a) 0.54Mn, 0.21Fe, (b) 0.02Mn, 0.09Fe, (c) 0.54Mn, 0.62Fe, (d) 0.02Mn, 0.63Fe, (e) 0.54Mn, 1.24Fe, (f) 0.02Mn, 1.19Fe, (g) 0.54Mn, 1.86Fe, (h) 0.02Mn, 1.82Fe.

confirmed as β-AlFe phase with the typical composition of β-$Al_{13}(Fe,Mn)_4Si_{0.25}$. In the alloy without Mn addition, as shown in Fig. 4h, a large fraction of the long needle-shaped primary Fe-rich intermetallics were found in the microstructure, which were confirmed by EDX as β-AlFe phase with the typical composition of β-$Al_{13}Fe_4$. Only a small fraction of Fe-rich intermetallic compounds were in the form of compact format, which was confirmed by EDX as α-AlFeSi phase with the typical composition of α-Al_8Fe_2Si.

In the as-cast microstructure, some coarse Fe-rich intermetallics developed into more complex morphologies such as star-like shapes in associated with primary α-Al phase, as shown in Fig. 5. These Fe-rich intermetallics have been found in the castings with experimental composition of Fe > 0.6 wt % and identified as α-AlFeMnSi phase with the typical composition of α-$Al_{24}(Fe,Mn)_6Si_2$. It was also found that the star-like α-AlFeMnSi phase were usually associated with α_1-Al phase formed in the shot sleeve. The results indicate that the solidification environments, especially the cooling rate in the

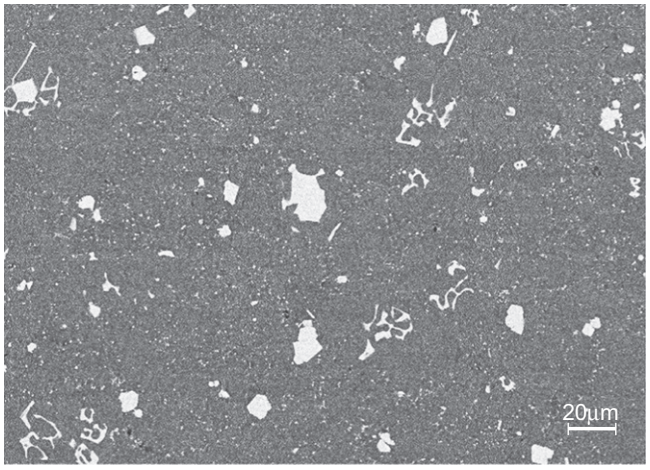

Fig. 5. Backscattered SEM micrograph showing the morphology of Fe-rich intermetallics in the diecast Al–5Mg–2Si alloy with 0.54Mn and 0.84Fe.

Table 2
Average compositions of Fe-rich intermetallic phases measured by quantitive SEM/EDX analysis.

Mn (wt.%)	Phase morphology	Identified compounds	Al	Fe	Mn at%	Si	Fe/Mn
0.54	Coarse compact	$Al_{24}(Fe,Mn)_6Si_2$	76.64	11.83	5.95	6.27	1.99
	Fine compact	$Al_{24}(Fe,Mn)_6Si_2$[a]	75.47	12.16	6.28	6.09	1.94
	Large needle	$Al_{13}(Fe,Mn)_4Si_{0.25}$	75.62	19.20	3.81	1.37	5.04
0.02	Fine compact	Al_8Fe_2Si[a]	35.01	9.59	–	4.13	–
	Large needle	$Al_{13}Fe_4$	75.50	24.51	–	–	–

[a] The composition was further confirmed by TEM/EDX analysis.

shot sleeve is capable of producing different morphologies of primary α-AlFeMnSi phase.

From these observations, the Fe-rich compounds of the compact and needle-shaped morphologies were identified as the α-AlFeMnSi (α-AlFeSi) and β-AlFe phase, respectively. The intermetallic compounds in the Al–Mg–Si alloys with and without Mn addition are summarised in Table 2. It is seen that the primary α-$Al_{24}(Fe,Mn)_6Si_2$ intermetallics formed in the die cavity were observed in all diecast alloys in the experimental range. However, the primary Fe-rich intermetallics formed in the shot sleeve were significantly affected by the Fe contents. It is noticeable that the intermetallic β-$Al_{13}(Fe,Mn)_4Si_{0.25}$ and β-$Al_{13}Fe_4$ phases formed in the experimental alloys were different to the intermetallic β-Al_5FeSi and β-AlFeSi phases observed in Al–Si, Al–Si–Cu and Al–Si–Mg alloys [9,18,20]. However, the cubic α-AlFeMnSi phase of α-$Al_{24}(Fe,Mn)_6Si_2$ intermetallics formed in the experimental alloys was found to be very similar to α-$Al_{15}(FeMn)_3Si_2$ intermetallics formed in Al–Si, Al–Si–Cu and Al–Si–Mg alloys [6,16,28].

In order to characterize the Fe-rich intermetallics in the alloys, their sizes and solid fractions were measured in the microstructure. The results for the fine α-AlFeMnSi and fine α-AlFeSi particles that are formed in the die cavity are shown in Fig. 6. Both particles followed a level correspondence to the Fe contents, which were consistently at 0.76 μm in diameter and no significant variation within the experimental ranges (Fig. 6a). The distribution of the fine Fe-rich particles was well matched by the normal distribution curve with an average of 0.76 (Fig. 6b). However, the volume fraction of the fine Fe-rich particles increased with the increase of Fe contents in the alloys (Fig. 6c). As the fine Fe-rich particles were formed during the solidification in the die cavity under high cooling rate, the results indicate that

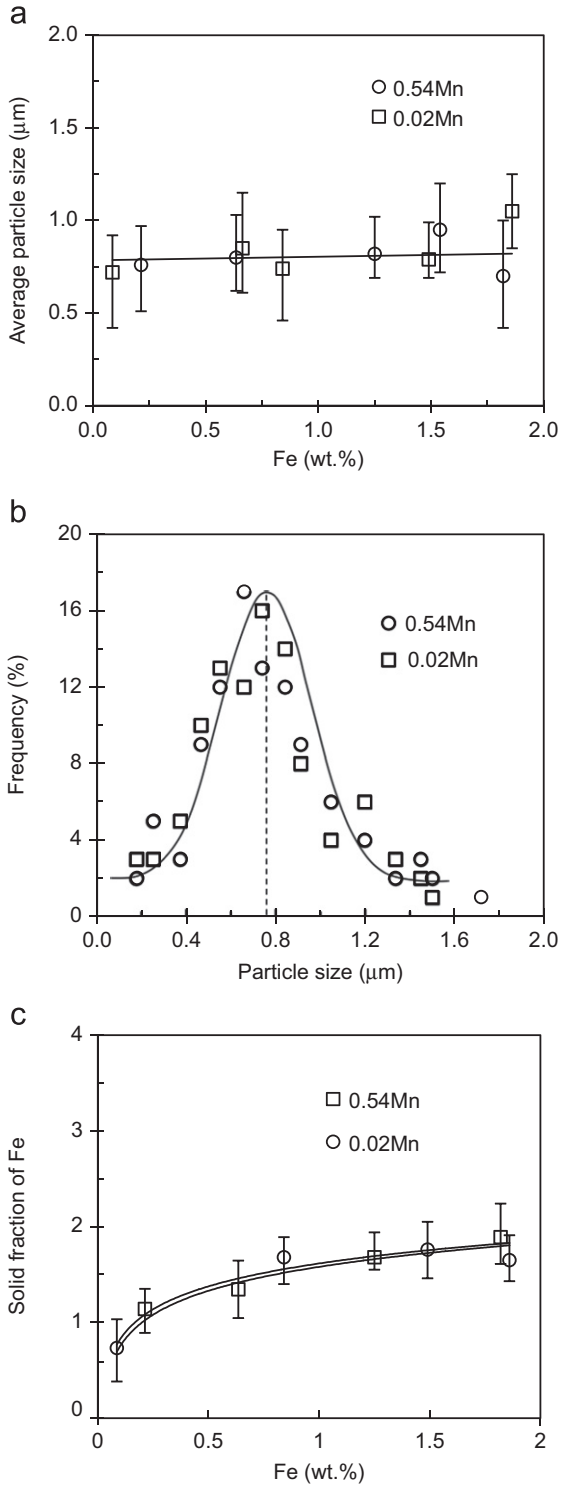

Fig. 6. Effect Fe contents in the diecast alloy on (a) the average size, (b) the frequency and (c) the volume fraction of Fe-rich intermetallic phase solidified in the die cavity.

the sizes of the Fe-rich intermetallics were mainly determined by the increased undercooling, enhanced heterogeneous nucleation and the shortened solidification time for the particle to grow.

In the Al–Mg–Si alloys with and without Mn addition, it is seen that the average sizes and volume fractions of the Fe-rich intermetallics solidified in the shot sleeve were obviously different to that formed in the die cavity, as shown in Fig. 7. The volume fraction and the size of the primary Fe-rich intermetallics

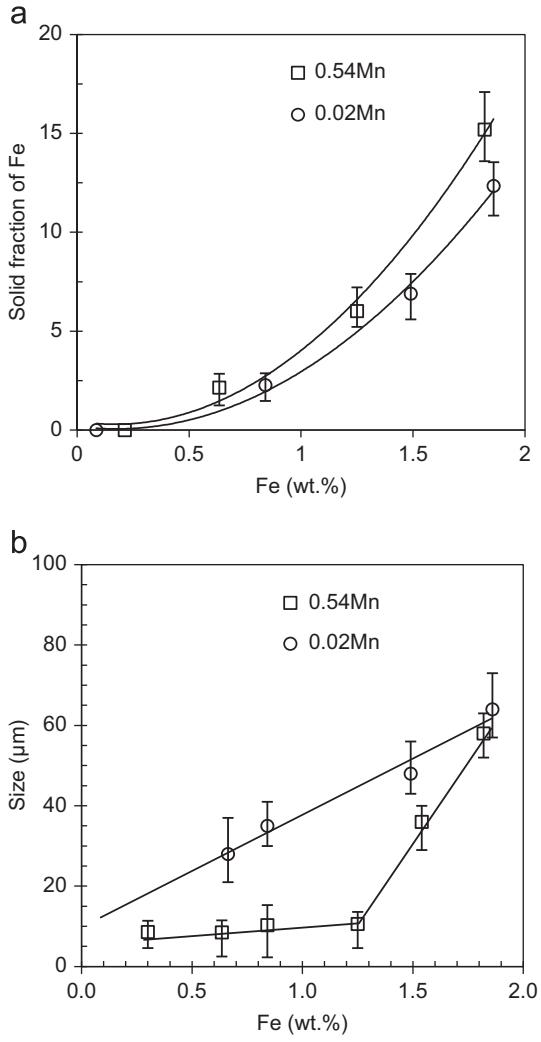

Fig. 7. Effect of Fe contents in the diecast alloy on (a) the volume fraction and (b) the average size of Fe-rich intermetallic phase solidified in the shot sleeve.

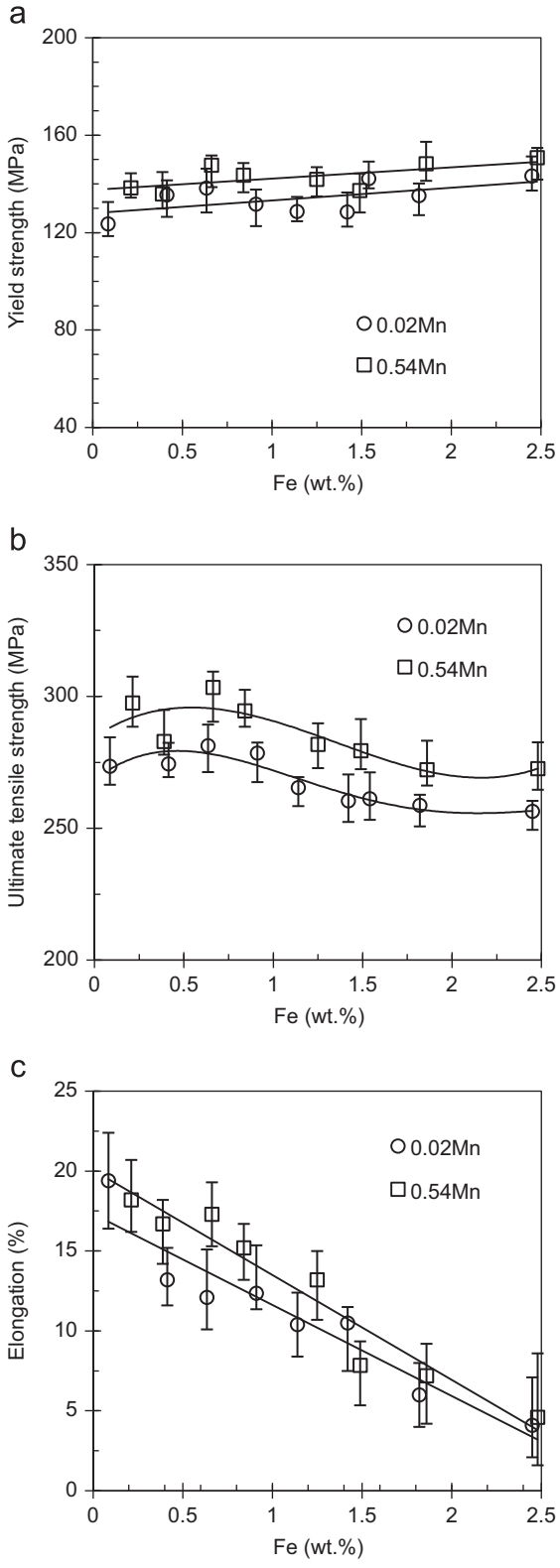

Fig. 8. Effect of Fe content on the mechanical properties of die cast Al–Mg–Si alloys with different amounts of Mn, (a) yield strength, (b) ultimate tensile strength, and (c) elongation.

increased significantly with the increase of Fe contents in the alloys. However, the size of the Fe-rich intermetallics increased in different ways. A linear increase of the size in the Fe-rich intermetallics was found in the alloys without Mn addition, but the size of Fe-rich intermetallics followed two separate linear correspondences to the Fe contents at a vertex of 1.24 in the alloy with Mn addition. A gradual increase was found at Fe < 1.24 wt% and a significant increase was found at Fe > 1.24 wt%. The vertex in Fig. 7b confirmed that the critical Mn/Fe ratio is at level of 0.5 to suppress the formation of β-$Al_{13}(Fe,Mn)_4Si_{0.25}$ in the alloys.

3.2. Mechanical properties

Mechanical properties of the diecast Al–Mg–Si alloys with different Fe and Mn contents are presented in Fig. 8. It is seen that a slight enhancement in the yield strength and a significant detrimental to the elongation with the increase of Fe contents in the alloys. However, no obvious variation in the ultimate tensile strength was observed until Fe was higher than 0.6 wt% where it decreased. Overall, the strength and the elongation of the diecast alloys with different Fe levels were all effectively higher in the alloys with 0.54 wt%Mn than these of their diecast counterparts with 0.02 wt%Mn. In addition to the slightly variation of Mg and Si concentrations in the alloys, as shown in Table 1, the difference in Mn content was one of the major factors to affect the strength and elongation of the diecast alloys. It is worth for a further emphasis that the enhancement of the yield strength for the diecast samples is less effective than the detrimental to the elongation of the same alloy in the experimental ranges.

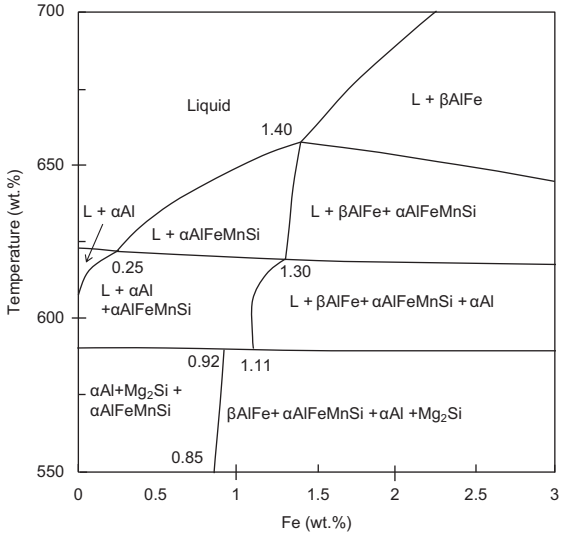

Fig. 9. Cross section of equilibrium phase diagram of Al–5Mg–2Si–0.6Mn–xFe calculated by Pandat software [29].

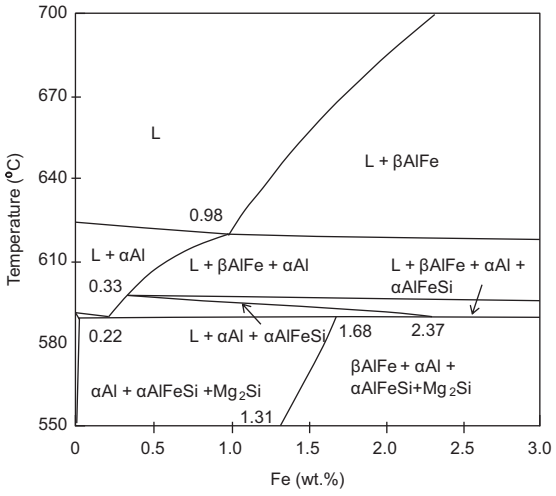

Fig. 10. Cross section of equilibrium phase diagram of Al–5Mg–2Si–xFe calculated by Pandat software.

The overall increase of the yield strength of the diecast sample was 8% while the ultimate tensile strength decreased by 9% and the elongation decreased by 295%.

3.3. CALPHAD of the multi-component Al–Mg–Si–Mn–Fe and Al–Mg–Si–Fe systems

In order to understand the effect of alloying on solidification and microstructural evolution, CALPHAD modelling of the multi-component Al–Mg–Si–Mn–Fe and Al–Mg–Si–Fe systems was carried out using PandaT software [29]. The Ti and other low levels of elements were not considered. The COST507 thermodynamic database [30] was used for constituent alloy systems and the α-AlFeMnSi was treated as a stoichiometric phase during the modelling. The calculated equilibrium phase diagrams on the cross sections of Al–5Mg–2Si–0.5Mn–xFe and Al–5Mg–2Si–xFe are shown in Figs. 9 and 10, respectively.

For the Al–Mg–Si–Mn–Fe system, the calculated diagram shown in Fig. 9 can be divided into several regions with different Fe contents. The phase formation follows: (1) L→α-Al+α-AlFe

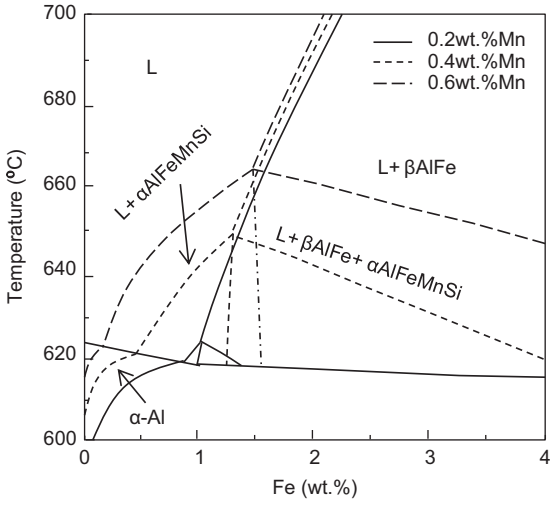

Fig. 11. Effect of Mn on the cross section of equilibrium phase diagram of Al–5Mg–2Si–xFe calculated by Pandat software.

MnSi+Mg_2Si with prior α-Al phase at Fe < (0.25 wt%), and (2) L→α-AlFeMnSi+α-Al+Mg_2Si with prior α-AlFeMnSi phase at 0.21 wt% < Fe < 1.4 wt%, and (3) L→β-AlFe +α-AlFeMnSi+α-Al+Mg_2Si with prior β-AlFe phase at Fe > 1.4 wt%. It needs to emphasise that the β-AlFe phase can be formed with a very low Fe content according the equilibrium phase diagram. However, the formation of β-AlFe phase in the as-cast microstructure of the experimental alloys with 0.54 wt%Mn is from 1.2 wt%Fe. The difference may be attributed to several factors including the noon-equilibrium solidification in HPDC process, the complex of precipitation process of intermetallics during solidification, and the database used in phase diagram calculation.

Similarly, for the Al–Mg–Si–Fe system shown in Fig. 10, the solidification procedure roughly follows: (1) L→α-Al+α-AlFe-Si+Mg_2Si with prior α-Al phase at Fe < (0.98 wt%), in which β-AlFe phase may exist at 0.22 wt% < Fe < 0.98 wt%, and (2) L→β-AlFe+α-AlFeSi+α-Al+Mg_2Si with prior β-AlFe phase at Fe > 0.98 wt%. The experimental results should that the β-AlFe phase was observed in the alloy with Fe content higher than 0.62 wt%.

The effect of Mn and Fe contents on the formation of Fe-rich intermetallic compounds are further demonstrated in Fig. 11 for the Al–Mg–Si alloys with three different levels of Mn contents at 0.2, 0.4 and 0.6 wt%, respectively. It is seen that the Fe content was lowered to form prior α-Al phase with the increases of Mn contents in the alloy. In other words, with the increase of Mn in the alloy, the α-AlFeMnSi was formed as prior phase at a lower level of Fe content in the alloy. Meanwhile, the addition of Mn also increased the Fe levels to form β-AlFe phase. Therefore, the area to form α-AlFeMnSi was significantly enlarged with the increase of Mn contents. This implies that the addition of Mn in the alloy can suppress the formation of β-AlFe intermetallic compounds in the alloy with practically possible high Fe content. On the other side, as seen in Fig. 11, the results confirmed that the increase of Mn in the alloy resulted in a significant increase of liquidus temperature of the alloy.

4. Discussion

4.1. Phase formation in diecast Al–Mg–Si alloy

The experimental observations have confirmed that (1) α-AlFeMnSi intermetallics can be formed in two solidification stages

during HPDC, one is in the shot sleeve and the other is in the die cavity, which show the compact morphology with different sizes; (2) manganese increases the Fe content range over which α-AlFeMnSi phase forms; (3) the Mn/Fe ratio at 0.5 is applicable to form β-AlFe intermetallics in the Al–Mg–Si–Mn alloy during HPDC; (4) no β-Al_5FeSi and β-AlFeSi intermetallics are observed in the Al–Mg–Si diecast alloys with varied Mn and Fe contents.

Generally, the phase formation of Fe-rich intermetallics in the experimental alloys is broadly consistent with the equilibrium phase diagram calculated from CALPHAD. Therefore the solidification path can be used to explain the major features of the microstructure. The solidification process and the associated changes of liquid compositions determine the formation of different phases. From the phase diagram in Fig. 9, it is seen that the prior phase is α-Al phase when Fe content is less than 0.25 wt%. The solidification starts to precipitate the α-Al phase in the shot sleeve, which is interrupted during die filling. The precipitation of α-Al phase continues in the die cavity, during which Si, Fe and Mn elements are enriched in the remaining liquid and the Fe-rich intermetallics are consequently formed in the melt. The high cooling rate in the die cavity and the absence of superheat in the melt enhance the heterogeneous nucleation, and therefore promote the formation of fine compact α-AlFeMnSi intermetallics. When Fe content is increased to a higher level, the prior phase becomes α-AlFeMnSi. The precipitation of α-AlFeMnSi compounds increases the undercooling in front of the interface of the crystal, resulting in the nucleation and growth of α-Al phase in associated with α-AlFeMnSi compounds (Figs. 2 and 4). The solidification continues in the die cavity, where the compact α-AlFeMnSi compounds and α-Al phase precipitate under high cooling rate. When Fe content is further increased, the prior phase is β-AlFe phase. The precipitation of β-AlFe compounds consumes Fe element in the melt and thus alters the local melt composition with enriched Si and Mn, resulting in an increase of Mn/Fe ratio. When Mn/Fe ratio reaches the limitation, α-AlFeMnSi compound precipitates from the melt. The following solidification precipitate the α-AlFeMnSi and β-AlFe compounds. Overall, the formation of α-AlFeMnSi and β-AlFe phases consumes Fe, Mn, Si prior to the eutectic solidification. The final stage of solidification of the alloys is the multi-eutectic transformation to generate the eutectic structure mainly of Al–Mg_2Si eutectic phase.

Mn is largely consumed by the formation of the Fe-rich intermetallics. Therefore, an adequate level of Mn is necessary in order to maintain high Mn/Fe ratio for the formation of the cubic α-AlFeMnSi phase. In the observed α-AlFeMnSi intermetallics, the typical composition is α-$Al_{24}(Fe,Mn)_6Si_2$, which is made of less Si than that in the common α-$Al_{15}(FeMn)_3Si_2$ compounds. The main reason can be attributed to the low Si concentration in the alloy and the short of Si supply during solidification. In the experimental results, it is also confirmed that Mn/Fe=0.5 is necessary to suppress the formation of the β-AlFe compounds in the as-cast microstructure. β-AlFe intermetallics is immediately observed in the alloys when Mn/Fe < 0.5, which is in good agreement with the observation in other alloys including Al–Si, Al–Si–Cu and Al–Si–Mg alloys [6–13]. However, α-AlFeMnSi phase can still be observed at low Mn/Fe ratio. Therefore, the Mn/Fe ratio can be used as an indicator for the formation of β-AlFe compounds, but not for determining the formation of α-AlFeMnSi phase.

The absence of β-Al_5FeSi intermetallics in the diecast Al–Mg–Si alloy is one important feature. In the equilibrium state, the β-Al_5FeSi intermetallics has a monoclinic crystal structure with the lattice parameters $a=b=0.612$ nm, $c=4.15$ nm, and $\beta=91^\circ$ [7] or $a=b=0.618$ nm, $c=4.15$ nm, and $\beta=91^\circ$ [31]. Similarly, the crystal structure of β-Al_3Fe and β-$Al_{13}Fe_4$ phase is also monoclinic with $a=1.549$ nm, $b=0.808$ nm, $c=1.248$ nm, $\beta=107.8^\circ$ [32]. Currently, it is still not clear for the conditions to form β-Al_5FeSi or β-Al_3Fe (β-$Al_{13}Fe_4$) in Al alloys. The effect factors are suspected in associated with the content of Fe and Si, in which low Fe contents and high Si/Fe ratio favour the formation of β-Al_5FeSi phase, but high Fe contents and low Si/Fe ratio tend to form β-Al_3Fe ($Al_{13}Fe_4$) phase [33]. Obviously, the more systematic work needs to address the mechanism in future.

4.2. Microstructure-property relationship

The experimental results have confirmed that the Fe-rich intermetallics significantly affect the mechanical properties of the Al–Mg–Si alloys. The higher the iron concentrations in the alloy, the significantly more the elongation decreases. This is accompanied by a slight enhancement of the yield strength at increased iron level in the alloys. The ultimate tensile strength maintains at similar level when Fe is less than 0.6 wt%, but it decreases significantly when the Fe contents further increases. Meanwhile, a slight enhancement of the yield strength is also observed in the alloy with Mn addition compare to that in the alloy without Mn addition.

Referring to the solidification microstructure, the enhanced yield strength is believed to correspond to the increased amounts of Fe-rich intermetallic compounds, especially the fine intermetallics present at the α-Al grain boundaries. The increase in yield strength is accompanied with decreasing elongation as the added reinforcement due to the Fe-rich compounds is at the cost of the alloy ductility. Therefore the detrimental effect of iron content on the mechanical properties in the diecast Al–Mg–Si alloys should be determined mainly by the loss in ductility.

Mn introduces an overall superiority in the elongation largely due to its effective role on modifying the morphologies and sizes of the primary Fe-rich intermetallic compounds. Long-needle shaped β-AlFe is either eliminated or modified into less harmful compact α-AlFeMnSi intermetallics by the Mn addition. Therefore, the elongation of the alloy with Mn addition is higher than that of their counterparts without Mn addition. However, the improvement of ductility vanishes in the alloys when Fe > 1.2 wt%, where large β-AlFe needles precipitate in the microstructure.

5. Conclusions

1) In high pressure die casting of Al–Mg–Si–(Mn) alloys, the formation of Fe-rich intermetallics occurs into two solidification stages. One is in the shot sleeve at lower cooling rates, and the other is in the die cavity at higher cooling rates. The Fe-rich intermetallics formed in the shot sleeve exhibit coarse compact, star-like or needle/plate shape morphology with varied sizes. The Fe-rich intermetallics formed in the die cavity are characterised by fine compact morphology with the size less than 3 μm.
2) In diecast Al–Mg–Si alloys, two types of Fe-rich intermetallics are formed over the Fe content range up to 2.4 wt %. The fine compact α-AlFeSi phase has the composition of α-Al_8Fe_2Si and the long needle β-AlFe phase has the composition of β-$Al_{13}Fe_4$. With 0.54 wt%Mn being added into the alloy, the fine compact intermetallic phase is found to be $Al_{24}(Fe,Mn)_6Si_2$ and the long needle β-AlFe phase is β-$Al_{13}(Fe,Mn)_4Si_{0.25}$.
3) In diecast Al–Mg–Si alloys containing 0.54 wt%Mn, the prior phase is α-Al when Fe is less than 0.21 wt%, but the prior phase is β-$Al_{13}(Fe,Mn)_4Si_{0.25}$ when Fe is higher than 1.24 wt%. Over the Fe contents range from 0.21 to 1.24 wt%, α-$Al_{24}(Fe,Mn)_6Si_2$ precipitates as prior phase to form either coarse compact

compounds in the shot sleeve or fine compact particles in the die cavity.

4) The morphology and size of α-$Al_{24}(Fe,Mn)_6Si_2$ intermetallics are dependent on the cooling rate. The higher cooling rate in the die cavity enables the α-$Al_{24}(Fe,Mn)_6Si_2$ phase to solidify in a fine compact morphology. However, the lower cooling rate in the shot sleeve results in the formation of compact and star-like Chinese script α-$Al_{24}(Fe,Mn)_6Si_2$ phase in the as-cast microstructure.
5) Fe-rich intermetallics significantly affect the mechanical properties of the alloy castings. The higher the iron concentrations in the alloy, the more significantly the ductility reduces. This is accompanied by a slight enhancement of the yield strength. The ultimate tensile strength maintains the similar level when Fe contents is less than 0.6 wt%, but decreases significantly with the further increase of Fe contents in the diecast alloys.
6) The yield strength and the ultimate tensile strength are slightly enhanced in the diecast Al–Mg–Si alloy when Mn is added in comparison with that without Mn addition.
7) Manganese promotes the formation of the cubic α-AlFeMnSi phase and suppresses the formation of β-AlFe phase in diecast Al–Mg–Si alloys. The β-AlFe compounds are formed when Mn/Fe ratio is less than 0.5.

Acknowledgement

The authors acknowledge the EPSRC and JLR for financial support.

References

[1] S. Ji, D. Watson, Z. Fan, M. White, Mater. Sci. Eng., A 556 (2012) 824–833.
[2] L. Wang, M. Makhlouf, D. Apelian, Int. Mater. Rev. 40 (1995) 221–238.
[3] J.L. Jorstad, Die Cast. Eng. (1986) 30–36. (Nov/Dec.
[4] Z. Yi, Y.X. Gao, P.D. Lee, T.C. Lindley, Mater. Sci. Eng., A 386 (2004) 396–407.
[5] G.B. Winkelman, Z.W. Chen, D.H. StJohn, M.Z. Jahedi, J. Mater. Sci. 39 (2004) 519–528.
[6] P. Skjerpe, Metall. Mater. Trans. A 18A (1987) 189–200.
[7] L.F. Mondolfo, Aluminium Alloys: Structure and Properties, Butterworth, London, 1976 534.
[8] L. Backerud, G. Chai, J. Tamminen, Solidification Characteristics of Aluminium Alloys, Foundry Alloys 2 (1990) 71–84. (AFS/Skanaluminum.
[9] S. Shivkumar, L. Wang, D. Apelian, JOM 43 (1991) 26–32.
[10] M.V. Kral, H.R. McIntyre, M.J. Smillie, Scr. Mater. 51 (2004) 215–219.
[11] J.G. Zheng, R. Vincent, J.W. Steeds, Philos. Mag. 79 (1999) 2725–2733.
[12] K.Y. Wen, W. Hu, G. Gottstein, Mater. Sci. Technol. 19 (2003) 762–768.
[13] A. Couture, AFS Int. Cast. Met. J. 6 (1981) 9–17.
[14] P.N. Crepeau, AFS Trans. 103 (1995) 361–366.
[15] D. Munson, J. Inst. Met. 95 (1967) 217–219.
[16] P. Hodgson, B.A. Parker, J. Mater. Sci. 16 (1981) 1343–1348.
[17] S.G. Shabestari, J.E. Gruzleski, Metall. Mater. Trans. 26A (1995) 999–1006.
[18] X. Cao, J. Campbell, Int. J. Cast Met. Res. 13 (2000) 175–184.
[19] C. Mascre, Fonderie 108 (1995) 4330–4336.
[20] X. Cao, J. Campbell, Metall. Mater. Trans. A 35A (2004) 1425–1435.
[21] G.K. Sigworth, S. Shivkumar, D. Apelian, AFS Trans. 97 (1989) 811–824.
[22] A. Pennors, A.M. Samuel, F.H. Samuel, H.W. Doty, AFS Trans. 106 (1998) 251–264.
[23] L.A. Narayanan, F.H. Samuel, J.E. Gruzleski, Metall. Mater. Trans. A 25A (1994) 1761–1773.
[24] S. Seifeddine, I.L. Svensson, Metall. Sci. Technol. (2009) 11–20 27-1-Ed.
[25] A.M. Samuel, A. Pennors, C. Villeneuve, F.H. Samuel, Int. J. Cast. Met. Res. 13 (2000) 231–253.
[26] X.P. Niu, B.H. Hu, S.W. Hao, J. Mater. Sci. Lett. 17 (1998) 1727–1729.
[27] E. Balitchev, T. Jantzen, I. Hurtado, D. Neuschütz, Calphad 27 (2003) 275–278.
[28] X. Fang, G. Shao, Y.Q. Liu, Z. Fan, Mater. Sci. Eng. A 445–446 (2007) 65–72.
[29] S.-L. Chen, S. Daniel, F. Zhang, Y.A. Chang, X.-Y. Yan, F.-Y. Xie, R. Schmid-Fetzef, W.A. Oatesd, Calphad 26 (2002) 175–188.
[30] I. Ansara, A.T. Dinsdale, M.H. Rand (Eds.), COST 507-Final Report: Thermodynamic Database for Light Metal Al-alloys, vol.2, European Communities, Brussels, 1998.
[31] R. Høier, O. Lohne, S. Mørtvedt, Scand. J. Metall. 6 (1977) 36–37.
[32] P. Skjerpe, J. Microsc. 148 (1987) 33–50.
[33] L. Sweet, S.M. Zhu, S.X. Gao, J.A. Taylor, M.A. Easton, Metall. Mater. Trans. A 42A (2011) 1737–1749.